J|A|C|S COMMUNICATIONS

Published on Web 05/06/2009

PtMo Alloy and MoO_x@Pt Core−Shell Nanoparticles as Highly CO-Tolerant Electrocatalysts

Zhufang Liu,[†] Jenny E. Hu,[‡] Qi Wang,[§] Karen Gaskell,[†] Anatoly I. Frenkel,[§] Gregory S. Jackson,[§] and Bryan Eichhorn*,[†]

Department of Chemistry and Biochemistry and Department of Mechanical Engineering, University of Maryland, College Park, Maryland 20742, and Department of Physics, Yeshiva University, New York, New York 10016

Received February 19, 2009; E-mail: eichhorn@umd.edu

In proton exchange membrane fuel cells (PEMFCs), pure Pt anode electrocatalysts are severely poisoned by trace amounts of CO that are ubiquitous in H_2 fuels derived from reformed hydrocarbons.[1] To circumvent this problem, bimetallic Pt−M electrocatalysts have been employed due to their higher CO tolerance compared to monometallic Pt nanoparticles (NPs).[2] Pioneering studies by Ross and Mukerjee have shown that PtMo alloys have exceptional low-temperature CO tolerance in both bulk electrodes and carbon-supported PtMo NP anodes.[3,4] However, solution-based syntheses of PtMo alloy NPs are particularly challenging due to the large negative redox potential of the Mo^{n+}/Mo^0 couple and the low miscibility of Pt and Mo. We have been developing solution-based routes to various bimetallic architectures (i.e., core−shell, alloy, aggregates) to compare their catalytic and electrocatalytic activities.[5] We describe here the solution-based synthesis and characterization of MoO_x@Pt core−shell and $Pt_{0.8}Mo_{0.2}$ alloy[4] NPs and their surprising CO-tolerant electrocatalytic activity.

$Pt_{0.8}Mo_{0.2}$ alloy NPs were prepared by the coreduction of $MoCl_3$ and $Pt(acac)_2$ in phenyl ether. Sodium triethylborohydride and oleic acid were employed as the reducing agent and capping agent, respectively. Figure 1a shows the transmission electron microscopy (TEM) image of 3.0 nm as-prepared $Pt_{0.8}Mo_{0.2}$ alloy NPs, which have a relatively narrow size distribution (Figure S1). The X-ray diffraction (XRD) profiles of the $Pt_{0.8}Mo_{0.2}$ alloy (Figure S2) show the expected[4a] face-centered cubic (FCC) lattice with $a = 3.91 \pm 0.01$ Å. The similarity to the 3.92 Å FCC cell of Pt is due to the nearly identical metallic radii of the two metals. Single-particle energy dispersive X-ray analysis (EDX) of $Pt_{0.8}Mo_{0.2}$ alloy NPs shows both Pt and Mo with an average atomic composition of 80% Pt and 20% Mo (Figure S3). In addition, the morphology and dispersity of the alloy particles are much different from those of monometallic FCC-Pt and body-centered cubic (BCC)-Mo NPs prepared under identical experimental conditions (Figure S4). To our knowledge, this is also the first solution-based synthesis of crystalline BCC-Mo NPs.

The oleic acid stabilized Mo NPs contain BCC-Mo (XRD) in the metallic state (X-ray photoelectron Spectrocopy (XPS)), however, the tightly bound oleic acid groups precluded the deposition of a Pt shell. As an alternative, a $NaBH_4$ reduction of $MoCl_3$ in ethylene glycol (EG) was employed in conjunction with the weakly coordinating polyvinylpyrrolidone (PVP) stabilizer. The "as-prepared" NPs are relatively monodispersed (∼3.5 nm) but are amorphous and oxidized (Figures S5, S6). XPS and X-ray Absorption Near Edge Structure (XANES) measurements are indicative of MoO_x NPs with mixed Mo(IV) and Mo(VI) oxidation states

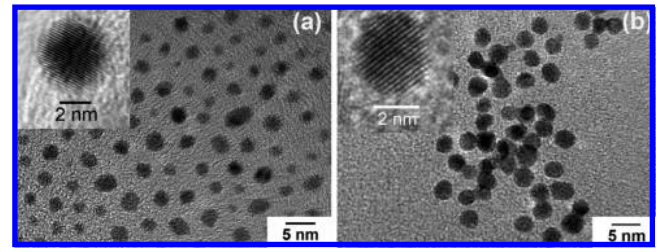

Figure 1. TEM image of (a) as-prepared PtMo alloy NPs and (b) MoO_x@Pt core−shell NPs. The insert is the HRTEM images of one particle.

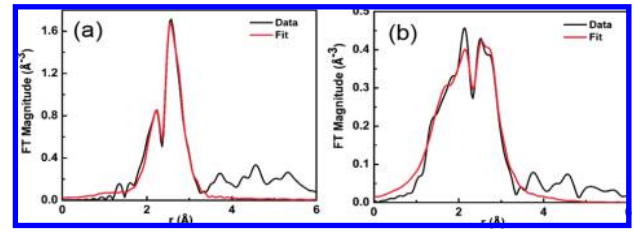

Figure 2. FT magnitudes of Pt L_3-edge data and fit for (a) MoO_x@Pt core−shell (k range from 2 to 19.8 Å) and (b) PtMo alloy (k range from 3.5 to 17.5 Å).

(Figure S7). However, the MoO_x NPs react directly with $PtCl_2$ in EG to give MoO_x@Pt core−shell NPs containing *ca.* 1−2 layers of Pt shells over MoO_x cores. The TEM image of the MoO_x@Pt core−shell NPs (Figure 1b) shows the ∼3.5 nm particles with a relatively narrow size distribution. The lack of a significant change in particle size and size distribution after the Pt deposition suggests a redox deposition process in which the outer layer of MoO_x NPs is replaced by 1−2 layers of Pt. The single-particle EDX analysis of 100 particles shows the MoO_x@Pt NPs have an average composition of 40% Pt and 60% Mo (Figure S8). The XRD profiles of the MoO_x@Pt NPs are dominated by diffraction of the Pt shells, which is also observed on related monolayer coated M@Pt systems with poorly crystalline cores.[5b,c]

Quantitative structural details of alloy and core−shell architectures were determined from extended X-ray absorption fine structure (EXAFS) studies. Visual examination of the raw Pt L_3-edge data (Figure 2) demonstrates dramatic differences between the two samples, in support of local structural rearrangements. Theoretical analysis was done by simultaneous Pt L_3- and Mo K-edge fits for the alloy (Mo K-edge data and fit are shown in Figure S10) and by a Pt L_3-edge fit for the core−shell sample (the Mo edge data for that sample could not be refined by the fitting analysis, possibly due to the highly disordered MoO_x core). The resultant Pt−Pt and Pt−Mo coordination numbers (5.1 ± 0.4 and 0.8 ± 0.4) in the PtMo alloy NPs correspond to the short-range order parameter of ca. 6 ± 3, i.e., consistent with the 80:20 Pt/Mo ratio and thus

[†] Department of Chemistry and Biochemistry, University of Maryland.
[‡] Department of Mechanical Engineering, University of Maryland.
[§] Yeshiva University.

10.1021/ja901303d CCC: $40.75

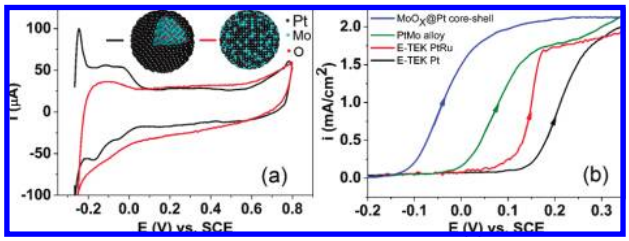

Figure 3. (a) CVs of the MoO_x@Pt core−shell and $Pt_{0.8}Mo_{0.2}$ alloy catalysts in 0.5 M H_2SO_4 at 298 K, scan rate 100 mV/s. (b) Polarization curves for oxidation of H_2 in the presence of 1000 ppm of CO on different catalysts (30% loading) at 298 K. Rotation rate: 1600 rpm. Scan rate: 1 mV/s. Before the potential scan, electrolytes were purged with the CO/H_2 mixture for 2 h at −0.20 V electrode potential. All the potential values given in the text are referred to the saturated calomel electrode (SCE).

indicative of a quasi-random alloy. In contrast, the MoO_x@Pt core−shell NPs show negligible Mo−Pt interactions (that were not required in EXAFS fits), a very disordered MoO_x core, and smaller bond length disorder than those in the $Pt_{0.8}Mo_{0.2}$ alloy. These data are indicative of a nonepitaxial, phase segregated Pt shell on an amorphous MoO_x core and are consistent with the TEM, XRD, XPS, and EDX data.

To prepare carbon-supported electrocatalysts (30 wt. % metal loading), the $Pt_{0.8}Mo_{0.2}$ alloy particles were loaded on VULCAN XC72 carbon by physical deposition from the colloidal suspension followed by heat treatment in Ar/H_2 (5% of H_2) atmosphere at 500 °C to remove the oleic acid. The NPs did not agglomerate or coalesce after high-temperature treatment (Figure S11), presumably due to the strong particle-support interactions. Carbon-supported MoO_x@Pt electrocatalysts were prepared similarly; however, thermal treatments were not required to activate the catalysts since PVP is only weakly bound to the particle surface (Figure S12). Room temperature cyclic voltammograms (CVs) in 0.5 M H_2SO_4 (Figure 3a) show distinct underpotential hydrogen adsorption/desorption (H_{upd}) peaks for the MoO_x@Pt catalysts that are characteristic of pure Pt surfaces.[6] However, the H_{upd} peaks are noticeably absent in the $Pt_{0.8}Mo_{0.2}$ alloy CV due to the alloyed surface.

The elecrocatalytic activity and CO tolerance of the NPs were evaluated using rotating disk electrode (RDE) experiments. As expected, both the $Pt_{0.8}Mo_{0.2}$ alloy and MoO_x@Pt core−shell electrocatalysts showed negligible overpotential for H_2 oxidation due to the presence of Pt on the NP surfaces (Figure S13). However, the polarization curves for oxidation of H_2 containing 1000 ppm of CO on MoO_x@Pt core−shell and $Pt_{0.8}Mo_{0.2}$ alloy NP electrocatalysts (Figure 3b) show markedly different behavior compared to commercial E-TEK Pt and PtRu alloy electrocatalysts at the same loadings. Interestingly, the MoO_x@Pt core−shell nanocatalysts show the lowest onset H_2 oxidation potential (−0.14 V), which is within the anode operation potential of PEMFCs. In addition, it reaches the diffusion-limited current at 0.1 V, which is far below that of Pt and PtRu. After potential cycling between −0.25 and 0.5 V for several hours in H_2SO_4, the H_2 oxidation onset potential rises and stabilizes at −0.10 V but is always superior to the $Pt_{0.8}Mo_{0.2}$ alloy and the PtRu catalysts. However, after heat treatment at 550 °C in Ar/H_2 atmospheres, the MoO_x@Pt catalyst phase segregates to MoO_x and pure Pt (Figure S14). The resulting CO tolerance is significantly diminished (Figure S15) and is comparable to that of the known Pt/MoO_x aggregate catalysts.[7] The H_2 oxidation onset for the $Pt_{0.8}Mo_{0.2}$ alloy starts at a higher potential than the MoO_x@Pt catalysts but still shows superior CO tolerance compared to both Pt and PtRu alloy catalysts.

It is generally accepted that the CO oxidation processes on Pt−M alloys occur by way of the "bifunctional mechanism" in which OH species adsorbed on the highly oxophilic Mo (or Ru) sites facilitate the oxidation of CO adsorbed on the Pt sites.[8,9] In contrast, the pure Pt surface of the MoO_x@Pt NPs requires a different mechanism of oxidation. It is likely that the electronic effect of the MoO_x core on Pt shell weakens the Pt−CO bond, which may dramatically reduce the oxidation overpotential.[2b,4b,c,10]

In conclusion, new synthetic strategies for PtMo alloy and MoO_x@Pt core−shell NPs were successfully designed and implemented. RDE results demonstrated that the MoO_x@Pt core−shell and $Pt_{0.8}Mo_{0.2}$ alloy NPs have substantially higher CO tolerance than both PtRu alloy and Pt catalysts. In addition, we have shown that PVP-capped NP colloids can be used directly in supported electrocatalyst assemblies without thermal pretreatment.

Acknowledgment. This work was supported by the DOE HFI program, Grant No. DE-FG02-05ER15731, the University of Maryland Energy Research Center (UMERC), and Department of Energy, Grant Nos. DE-FG02-03ER15476 and DE-FG02-05ER15688 (to A.I.F.). We thank Dr. Selim Alayoglu for helpful discussion.

Supporting Information Available: Detailed procedures for NP synthesis; full XRD, TEM, XPS, EXAFS, and electrochemical characterizations. This material is available free of charge via the Internet at http://pubs.acs.org.

References

(1) Wee, J. H.; Lee, K. Y. *J. Power Sources* **2006**, *157*, 128.
(2) (a) Lee, S. J.; Mukerjee, S.; Ticianelli, E. A.; McBreen, J. *Electrochim. Acta* **1999**, *44*, 3283. (b) Tong, Y. Y.; Kim, H. S.; Babu, P. K.; Waszczuk, P.; Wieckowski, A.; Oldfield, E. *J. Am. Chem. Soc.* **2002**, *124*, 468. (c) Brankovic, S. R.; Wang, J. X.; Adzic, R. R. *New Mater. Electrochem. Syst.* **2001**, *4*, A217. (d) Abe, H.; Matsumoto, F.; Alden, L. R.; Warren, S. C.; Abruna, H. D.; DiSalvo, F. J. *J. Am. Chem. Soc.* **2008**, *130*, 5452.
(3) (a) Grgur, B. N.; Zhuang, G.; Markovic, N. M.; Ross, P. N. *J. Phys. Chem. B* **1997**, *101*, 3910. (b) Grgur, B. N.; Markovic, N. M.; Ross, P. N. *J. Phys. Chem. B* **1998**, *102*, 2494.
(4) (a) Grgur, B. N.; Markovic, N. M.; Ross, P. N. *J. Electrochem. Soc.* **1999**, *146*, 1613. (b) Mukerjee, S.; Lee, S. J.; Ticianelli, E. A.; McBreen, J.; Grgur, B. N.; Markovic, N. M.; Ross, P. N.; Giallombardo, J. R.; De Castro, E. S. *Electrochem. Solid-State Lett.* **1999**, *2*, 12. (c) Mukerjee, S.; Urian, R. C.; Lee, S. J.; Ticianelli, E. A.; McBreen, J. *J. Electrochem. Soc.* **2004**, *151*, A1094.
(5) (a) Zhou, S.; Varughese, B.; Eichhorn, B.; Jackson, G.; McIlwrath, K. *Angew. Chem., Int. Ed.* **2005**, *44*, 4539. (b) Alayoglu, S.; Nilekar, A. U.; Mavrikakis, M.; Eichhorn, B. *Nat. Mater.* **2008**, *7*, 333. (c) Alayoglu, S.; Eichhorn, B *J. Am. Chem. Soc.* **2008**, *130*, 17479.
(6) Luo, J.; Wang, L.; Mott, D.; Njoki, P. N.; Lin, Y.; He, T.; Xu, Z.; Wanjana, B. N.; Lim, I. I. S.; Zhong, C. J. *Adv. Mater.* **2008**, *20*, 4342.
(7) Ioroi, T.; Yasuda, K.; Siroma, Z.; Fujiwara, N.; Miyazaki, Y. *J. Electrochem. Soc.* **2003**, *150*, A1225.
(8) Watanabe, M.; Motoo, M. *J. Electroanal. Chem.* **1975**, *60*, 275.
(9) Gasteiger, H. A.; Markovic, N.; Ross, P. N.; Cairns, E. J. *Electrochim. Acta* **1994**, *39*, 1825.
(10) (a) Davies, J.; Hayden, B. E.; Pegg, D. J. *Electrochim. Acta* **1998**, *44*, 1181. (b) Igarashi, H.; Fujino, T.; Zhu, Y. M.; Uchida, H.; Watanabe, M. *Phys. Chem. Chem. Phys.* **2001**, *3*, 306. (c) Watanabe, M. Design of Electrocatalysts for Fuel cell. In *Catalysis and Electrocatalysis at Nanoparticle Surface*; Wiechowski, A., Ed.; Marcel Dekker Inc.: 2003; pp 827−846. (d) Watanabe, M.; Zhu, Y. M.; Uchida, H. *J. Phys. Chem. B* **2000**, *104*, 1762.

JA901303D